Feature-Oriented Acoustic Tomography for Coastal Ocean Observatories

Olivier Carrière and Jean-Pierre Hermand, *Fellow, IEEE*

***Abstract*—The deployment of coastal observatories motivates the development of acoustic inversion schemes able to characterize rapidly time-varying range-dependent environments. This paper develops feature models as parameterization schemes for the range-dependent temperature field, when the latter is mainly influenced by an identified oceanic feature, here thermal fronts. The feasibility of feature-oriented acoustic tomography (FOAT) is demonstrated in two cases of coastal thermal front known to occur regularly: the Ushant tidal front, France (48.5° N, 5° E), and the Cabo Frio coastal upwelling, Brazil (23° S, 42° W). Realistic scenarios simulated with regional circulation models provide typical environmental variations for testing the validity of the FOAT approach, with both global optimization and sequential filtering of the (synthetic) full-field acoustic data. Matched-field processing at multiple frequencies is used to reduce ambiguities between parameters and to achieve a good tradeoff between robustness and sensitivity. The proposed feature-model parameterization is shown to provide robust estimates of the 2-D temperature field even when the simulated environment presents smaller scale inhomogeneities. Moreover, the sequential filtering based on a random walk model of the thermal front parameters enables a stable tracking of typical temperature field variations along several days. This sequential approach is particularly convenient for continuous, long-term monitoring operated with bottom-moored ocean observatories.**

***Index Terms*—Coastal acoustic tomography, inversion, Kalman filter, random walk, range dependent, sequential Bayesian filtering, thermal front, upwelling.**

I. Introduction

THE deployment of coastal observatories is an excellent opportunity for continuous acoustic tomography installations. Ocean acoustic tomography (OAT) can provide additional measurements to supplement the observations available for data assimilation[1] [1], [2]. Coastal environments are often characterized by strongly range-dependent structures, induced by topography, winds, or tidal currents. In this case, the range-integrated tomography techniques are irrelevant and specific range-dependent parameterization schemes must be developed. In this paper, feature models (FMs) are used as parameterization schemes for the 2-D temperature field of vertical slices of the environment, to enable the acoustic inversion and tracking of relevant oceanic features (here, thermal fronts) with temporal and spatial scales suitable for their assimilation in regional oceanic circulation models.

OAT was introduced at the end of the 1970s as an efficient tool to monitor the range-averaged sound-speed profile along the propagation path of transmitted acoustic waves [3]. One of the essential problems in OAT and, more generally, in inverse problems, is the parameterization of the observed system. In ocean acoustic tomography, a well-known choice is the empirical orthogonal functions (EOFs) [4]. Provided that historical databases or accurate oceanographic predictions are available, the EOFs constitute a basis of functions on which any sound-speed profile can be projected, therefore reducing the parameter space dimension to the number of EOFs taken into account.

When the use of a network of source and receivers is not possible, the recovery of range-dependent properties of the sound-speed field by vertical slice tomography is a complex task, since the uniqueness of the solution is not guaranteed. A straightforward approach is to divide the 2-D sound-speed field into several range-independent subsections parameterized individually, e.g., with EOFs. This approach has been proposed in different works [5]–[8] showing that the range dependence of a 2-D sound-speed field can be characterized by vertical slice tomography if constraint or regularization are involved in the inversion scheme.

In this paper, a different approach is developed, based on a parameterization dedicated to specific oceanographic features that are expected to occur in the probed environment. Contrary to the range-discretization approach, the present method involves a reduced parameter set that determines the global structure of the 2-D temperature field. With such an approach, the aim is not to solve small-scale features or inhomogeneities, but to identify the main oceanographic features and to track their evolution in time. Therefore, this method is dedicated to situations where the sound-speed field is strongly determined by a known oceanographic feature (front, eddy).

[1]Data assimilation is the generic title of mathematical or numerical methods for combining observations efficiently with a model.

Manuscript received March 16, 2011; revised December 07, 2011 and July 19, 2012; accepted October 29, 2012. Date of publication January 03, 2013; date of current version July 10, 2013. This work was supported by the Fonds pour la formation à la Recherche dans l'Industrie et dans l'Agriculture (FRIA); the Fonds de la Recherche Scientifique (FNRS), Belgium; the European Seas Observatory Network (ESONET) Network of Excellence and Ocean Acoustic Exploration IRSES (OAEx); the European 6th and 7th Framework Programs; the European Commission; and the Service Hydrographique et Océanographique de la Marine Française (SHOM) under SINOBAD Project.

Associate Editors: W. M. Carey and J. F. Lynch.

O. Carrière was with the Acoustics & Environmental Hydroacoustics Lab, LIST, École Polytechnique, Université libre de Bruxelles (ULB), Brussels B-1050, Belgium. He is now with the Marine Physical Laboratory, Scripps Institution of Oceanography, La Jolla, CA 92093-0238 USA (e-mail: ocarriere@ucsd.edu).

J.-P. Hermand is with the Acoustics & Environmental Hydroacoustics Lab, LIST, École Polytechnique, Université libre de Bruxelles (ULB), Brussels B-1050, Belgium (e-mail: jhermand@ulb.ac.be).

Color versions of one or more of the figures in this paper are available online at http://ieeexplore.ieee.org.

Digital Object Identifier 10.1109/JOE.2012.2227543

Here, the discussion is centered on the temperature field parameterization, assuming a known salinity and a negligible effect of the currents. Practically, inversion results typically provide the effective sound-speed field that combines the temperature and salinity fields, perturbed by the current component in the direction of the acoustic propagation. Therefore, such estimates have to be assimilated in circulation models to be properly integrated as an environmental measurement.

Oceanic models as well as simplified front models have been used to study the effect of fronts on acoustic propagation [9]–[13], with the general conclusions that the front properties strongly affect the transmission loss (positively or negatively), the ray travel times, and the coupling between propagation modes. Higher acoustic frequencies are typically more sensitive to temperature variations and exhibit more mode coupling. FMs are appropriate tools to study the relationship between front properties and acoustic propagation characteristics, since they consist of simple mathematical expressions that reproduce expected oceanographic features, parameterized with only the main properties of the feature (position, strength, etc.). It was shown in [14] that FMs can also provide significant improvement on the prediction of acoustic transmission loss (TL) with respect to range-independent models.

FMs were initially developed for oceanic modeling and data compression purposes. They are used for assimilation of observational data (satellite or *in situ* measurements) and also for multiscale analysis and simulation of complex regional ocean [15], [16]. Having this in mind, the proposed use of FMs for acoustic inversion can facilitate the assimilation of the resulting estimates in ocean models or substitute usual satellite observations of thermal fronts in case of subsurface feature or cloud cover.

The approach is demonstrated here on two particular cases of coastal thermal fronts. The first one is the so-called Ushant tidal front (48.5° N, 5° E) that takes place in the Iroise sea, France, during the northern summer. The study of this front is relevant for understanding small-scale mixing processes, and its accurate modeling requires a significant amount of observational data. The tracking of its position is also important for fisheries. The second thermal front is caused by the upwelling of South Atlantic Central Water (SACW) that climbs the shelf break near Cabo Frio, Brazil (23° S, 42° W). This feature is frequently observed during the austral summer and is known to interact with the other processes of the Brazilian Current (BC) system [17]. The acoustic data are synthesized from realistic oceanic simulations given by the HYbrid Coordinate Ocean Model (HYCOM [18]) for the Iroise sea tidal front, and the Regional Ocean Model System (ROMS [19]) for the Cabo Frio coastal upwelling.

Two different configurations are tested: the Ushant tidal front is tracked with an acoustic setup that corresponds to the deployment of a shore-cabled observatory equipped with a bottom-moored array of hydrophones, and a shallow acoustic source that mimics ship machinery noise with an acoustic center at a depth of a few meters. The ship traffic is intensive in this region, with two important and well-surveyed merchant traffic lanes. Most ships can constitute a source of opportunity with some *a priori* knowledge about their noise characteristics which can be deduced by combining traffic information given by the Maritime Rescue Co-ordination Centers (MRCC) and a suitable acoustic database. The feasibility of using the noise radiated by a ship as an opportunity source has been already demonstrated for acoustic tomography and geoacoustic inversion purposes [20]–[22]. This suggests that deployment of a passive acoustic tomography network in areas with intense traffic is pertinent and worth being examined in detail [23]. A significant amount of such passive data recorded recently in the Ushant area is already available for testing the feasibility of the approach in real situations. The upwelling feature of Cabo Frio is tracked with an opposite configuration. The acoustic source is placed inshore for maintenance facilitation and the hydrophone array is located offshore. This configuration enables consideration of the use of a thermistor string at the source location to constrain the upwelling FM.

Practically, the use of a dense array of hydrophones spanning the whole water column is not realistic. A reduction in the number of hydrophones and of the vertical extent can be compensated by an increase of transmitted frequencies, maintaining the total number of effective measurements. Several works have shown experimentally that broadband approaches enable consideration of a very sparse array (four hydrophones or less) [24]–[26]. It is worth noting that an increase of the number of frequencies has a nonnegligible impact on the computational burden due to the required fine grid of acoustic propagation. However, this computational cost increase is certainly preferable to the technical constraints and maintenance costs of large and dense arrays.

The remainder of this paper is organized as follows. Section II describes the Ushant tidal front and the Cabo Frio upwelling front and details the feature models used in the respective acoustic inversion problem. Section III investigates the problem of acoustic modeling for such strongly range-dependent coastal sound-speed field and illustrates the sensitivity of the conventional space-coherent matched-field processing (MFP) to FM parameters for the upwelling case. The section ends with a brief description of global optimization and sequential filtering algorithms used in this paper. Sections IV and V present the simulation results for the sequential tracking of the Ushant tidal front and for the inversion and sequential tracking of the Cabo Frio coastal upwelling, respectively. The paper is concluded in Section VI.

II. Thermal Front Feature Models

FMs are mathematical expressions that aim to reproduce oceanographic features with a reduced number of variables. Typically they require a limited number of vertical profiles (temperature, salinity, or sound speed) and a "melt" function that describes the rates of variation between these profiles. The melt function usually relies on physical parameters of the modeled feature (position, shape, width, etc.).

A. Ushant Tidal Front

The Ushant front is a tidal front which occurs off the Brittany coast (48.5° N, 5° E). It is characterized by the presence of homogeneous water near the coast and stratified water off the shore. The former results from an intense mixing due to tidal currents which are generally strong in the area. The Ushant

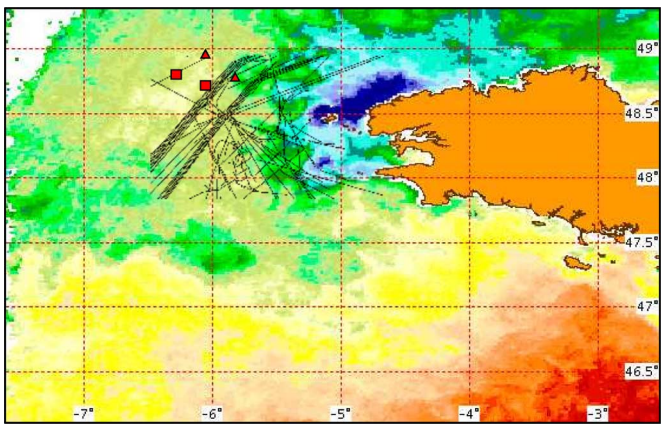

Fig. 1. Advanced very-high-resolution radiometer (AVHRR) satellite measurement in the Ushant front zone on August 11, 2007. The surface temperature field varies from 15.1 °C (dark blue) to 21.2 °C (dark red) [source: IFREMER, Satellite Application Facility (SAF) O&SI from EUMETSAT/Météo-France in Lannion, France]. The black solid lines show real data from ship trajectories along the Ushant traffic lanes [courtesy of G. Hajduk, Boost Tech., satellite image provider: European Space Agency (ESA)]. The positions of the autonomous underwater recorder for acoustic listening (AURAL) autonomous hydrophone deployed by SHOM during one month in 2009 (squares) and 2010 (triangles) are depicted in red [28].

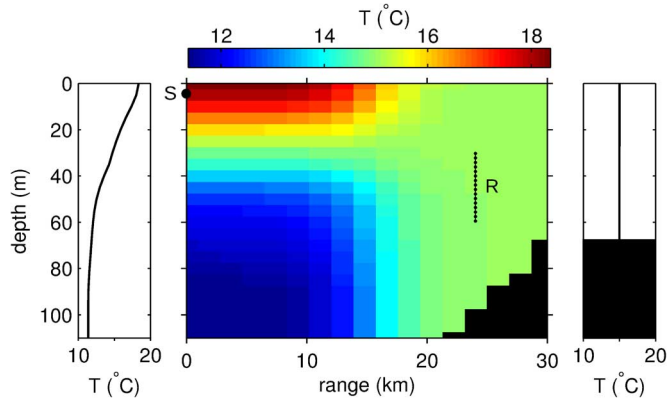

Fig. 2. Ushant thermal front. Example of temperature field constructed with the Ushant thermal front FM. The central position r_0 of the front is 15 km and the quarter length L equals 4 km. The stratified profile is given by the mean profile of the EOF database (see Fig. 3). The source (S) and 16-element receiver (R) setup involved in the simulations is depicted.

front is highly dynamic, generating a lot of meanders and moving with the tidal cycle for several tens of kilometers. It appears in mid spring and disappears in early fall. Climatological studies show that there is a 70% probability of observing it during northern summertime [27]. During this period, the surface temperature equals 18 °C–19 °C for the stratified water (offshore) and falls to 16 °C or less for the homogeneous part (inshore).

Satellite imagery enables the localization of the front. Fig. 1 shows an example of sea-surface temperature (SST) measurement in the front zone during summer. However, the frequent cloud cover in this region does not enable the use of satellite imagery as a permanent monitoring tool.

The Ushant front is idealized here with an FM that describes the temperature field $F(r, z)$ as a function of the horizontal distance r and the depth z. The thermal front FM is constructed as follows [14]:

$$F(r,z) = F_c(z) + \frac{F_h(z) - F_c(z)}{1 + e^{-2(r-r_0)/L}} \tag{1}$$

where $F_c(z)$ and $F_h(z)$ are the temperature profiles in the cold side and the hot side of the front, respectively, L is the quarter length of the front, and r_0 is the central position of the front defined by the maximum of the temperature gradient. An example of a typical temperature field obtained with the FM is shown in Fig. 2.

In this paper, an environmental scenario is simulated with HYCOM [18]. This model is a primitive equation ocean general circulation model that evolved from the Miami Isopycnic-Coordinate Ocean Model (MICOM [29]). Its adaptation to regional modeling has been realized by SHOM in the framework of the MOUTON project [30] with different improvements for more stable numerical scheme and boundary forcing suitable for coastal environment modeling. The resulting model has been validated by comparing simulation results and satellite or *in situ* measurements for different coastal areas with a horizontal resolution of about 2 km [31]. Initialization and boundary oceanic forcing is provided by global systems Mercator-Océan and MOG2D, while atmospheric forcings are from ARPEGE system of Météo-France.

A single vertical slice crossing the Ushant front is extracted from a simulation of the English Channel/Biscay system. Forty eight hours of 2-D temperature variations constitute our (hidden) scenario. Six parameters are retained for the FM parameterization: the front central position (r_0), the front quarter length (L), three empirical orthogonal function (EOF) coefficients to parameterize the stratified (hot) temperature profile (F_h) and one temperature value for the cold temperature profile (F_c), assumed to be isotherm. Using an EOF decomposition, every stratified profile $F_h(z)$ can be parameterized by a set of EOF coefficients α_j, $j = 1, \ldots, N$, following [4]:

$$F_h(z) = \overline{T(z)} + \sum_{j=1}^{N} \alpha_j \delta T_j(z) \tag{2}$$

where $\overline{T(z)}$ is the mean profile of the database and $\delta T_j(z)$ are the related EOFs. The mean profile and first three EOFs are shown in Fig. 3. The database is constructed here from the HYCOM temperature modeling outputs at the offshore location.

The 48-h evolution of the six parameters that best fit the HYCOM temperature modeling outputs [minimum range- and depth-averaged root mean square error (RMSE)] are shown in Fig. 12. The RMSE oscillates between 0.3 °C and 0.5 °C. In point of fact, the inshore part of the temperature field is not perfectly modeled by an isotherm. Therefore, the large values obtained for the front length parameter extend the stratification up to the cold part of the transect (inshore). The corresponding cold temperature parameter cannot be directly associated to the true temperature of the environment and can be seen as a virtual cold profile outside the transect bounds.

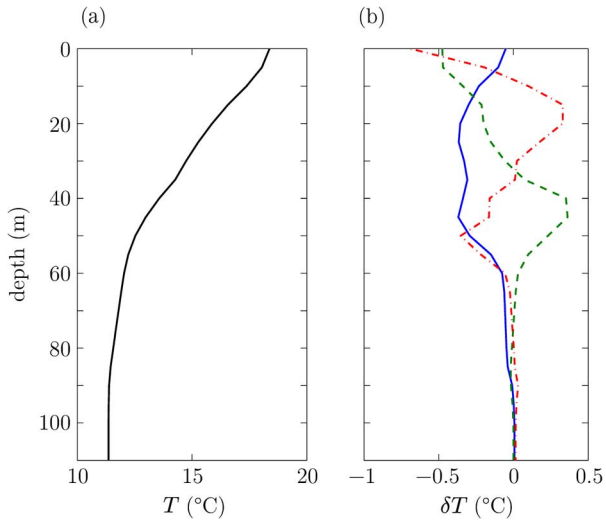

Fig. 3. Ushant thermal front. (a) Mean profile of the HYCOM temperature profiles at the defined offshore location. (b) First three EOFs of the database (solid blue line: EOF 1; dashed green line: EOF 2; dashed–dotted red line: EOF 3).

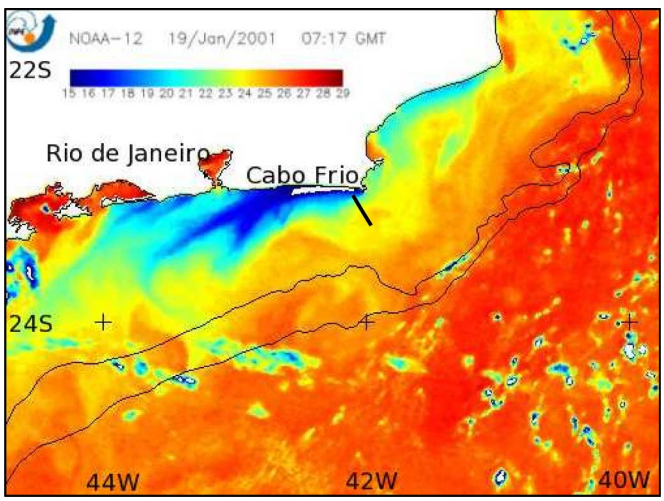

Fig. 4. AVHRR image from January 10, 2001 exemplifying the coastal upwelling in Cabo Frio region. The blueish-yellow colors are associated with the cooler and fresher coastal water on the shelf, and the reddish colors mark the presence of the warmer and saltier tropical water. The black line indicates the position of the transect involved in the simulations. Image courtesy of W. Lins de Mello, Brazilian Navy (reproduced from [34]).

B. Cabo Frio Coastal Upwelling

The upwelling phenomenon is defined by the rising of deep cold waters toward the surface, developing a thermal front. This particular feature is observed in Cabo Frio (23° S, 42° W; Fig. 4). Different mechanisms support or interact with the upwelling, including the Ekman pumping, the topography, and other specific oceanic structures, notably the BC front [16], [32], [33]. During the austral summer months, when coastal upwelling is more frequent and sustained due to favorable wind conditions over the Cabo Frio region, the surface temperature difference between offshore area and upwelled waters near the coast is mostly greater than 10 °C.

A schematic representation of the proposed FM structure for the upwelling region near Cabo Frio is shown in Fig. 5. It is derived from the continental shelf-slope front FM and thermal front FM developed in [15] and [14], and updated in [35] and [16], respectively. The upwelling front temperature distribution $T(r,z)$ in a 2-D vertical slice is parameterized as

$$T(r,z) = T_o(z) + m(r)\,[T_i(z) - T_o(z)] \tag{3}$$

where r and z are the horizontal and vertical coordinates, respectively, and $m(r)$ is the *melt* function. This function has to vary between 0 and 1 along the range to make the intermediate vertical temperature profiles gradually vary from $T_o(z)$ to $T_i(z)$. The melt function combines here the hyperbolic tangent and a nonlinear grid over which this hyperbolic tangent is computed. More precisely, the function is defined as

$$m(r;a) = \frac{1}{2} + \frac{1}{2}\tanh\left(2\pi\left(\frac{r}{R}\right)^{10^a} - \pi\right) \tag{4}$$

where R is the length of the simulated transect and a is the *melt parameter* that varies typically over the interval $[-1.5, 1.5]$. Practically, this melt function enables simulation of different positions for the maximum temperature gradient (the maximum value of the derivative of the melt function). The different shapes of the resulting melt function are plotted in Fig. 5(b).

Typically, the FM does not depend on bathymetric variations. However, in the present case of coastal upwelling, it is observed that isotherms follow roughly the slope of the bathymetry. Therefore, this feature is introduced in the geometric construction of the FM, in the following manner: the temperature field is first constructed as for a flat bottom, using (3), with a regular vertical (and horizontal) grid. Then, the vertical grid is compressed, as for sigma coordinates, to follow the bathymetry gradually. This transformation is outlined in Fig. 6.

As for the Ushant environment, realistic oceanic field variations are simulated from a regional circulation model. In this case, the scenario is simulated with ROMS [19]. This model solves the primitive equations of motion using S-coordinates vertically, allowing variable resolution mainly for the surface and bottom Ekman layers. The domain consists of ≈1-km horizontal resolution and 25 vertical levels and is limited geographically by 23°40′ S–22°20′ S and 42°50′ W–41°20′ W. Initial field conditions are given by climatological data and the oceanic forcing is deduced from time interpolation of the same data. Wind stress is provided by the National Centers for Environmental Prediction (NCEP) data [36].

Again, a vertical slice of the simulation that crosses the front is extracted to provide the test case. With known $T_i(z)$ and $T_o(z)$ profiles, the RMSE between ROMS modeling outputs and FM representation varies between 0.15 °C and 0.85 °C on the whole data set. This error can be slightly reduced by allowing the temperature profiles to vary. However, the forcing of at least one profile enables constraint of the inverse problem and favors a solution which is physically acceptable.

Ideally, the two extreme profiles $T_i(z)$ and $T_o(z)$ should be monitored to constrain the FM. Practically, however, monitoring the offshore temperature profile component is a difficult and costly task, while the use of a thermistor string in the shallowest part is reasonable to envision. To parameterize the offshore profile $T_o(z)$, a database of synthetic profiles is

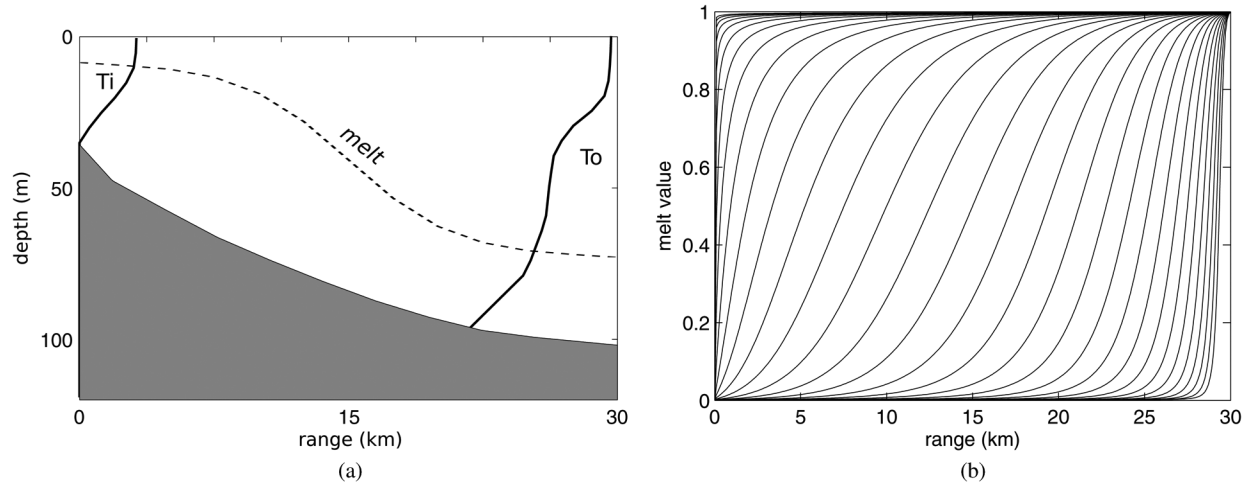

Fig. 5. Cabo Frio upwelling. (a) A schematic representation of the upwelling FM structure and its parameters. (b) Shape of the proposed melt function when varying the melt parameter a in the interval $[-1.5, 1.5]$.

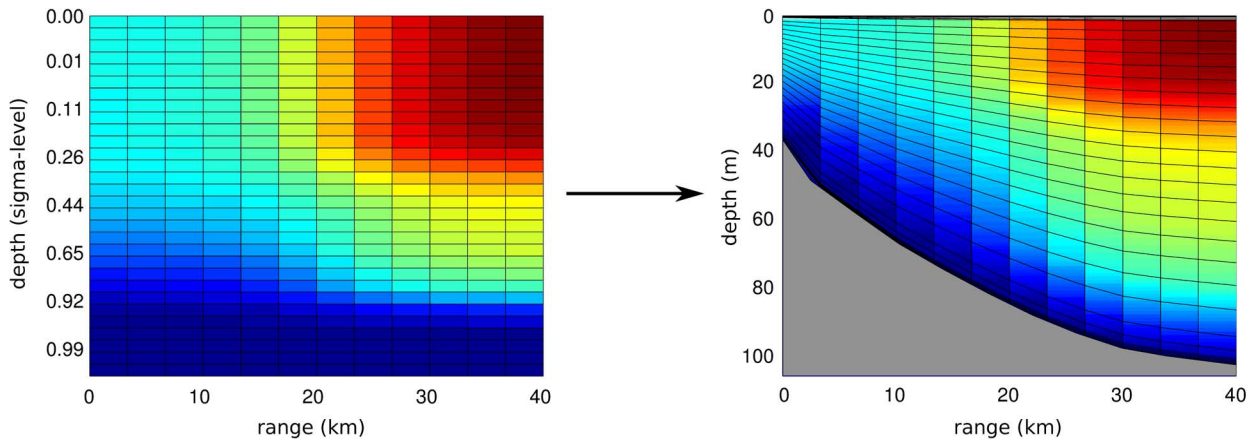

Fig. 6. Cabo Frio upwelling. A scheme of the sigma-coordinate technique in the upwelling FM construction. The original FM is expressed on a sigma-coordinate grid and then compressed progressively with the bathymetry.

constructed with the whole set of offshore profiles given by the oceanic numerical model and decomposed in an EOF basis. Fig. 7 shows the mean profile and the first three EOFs obtained from ROMS predictions.

It is worth noting that the shape of the melt functions (hyperbolic tangent or exponential forms) avoids introducing inhomogeneities between the two extreme profiles. While it is still possible to refine the melt function, a higher complexity comes at the expense of a higher number of parameters, which is not desirable for the purposes of the approach.

III. Feature-Oriented Acoustic Tomography

A. Acoustic Modeling in a Highly Range-Dependent Environment

When dealing with range-dependent situations (bathymetry, sound-speed field, or bottom geoacoustic parameters), parabolic equation and coupled normal mode models are required to properly predict the acoustic complex pressure field [37]. In the present study, the acoustic modeling takes into account the range-dependent bathymetry and the bottom acoustic properties. The sea bottom of the Ushant environment is modeled as a half-space composed of gravel (compression wave speed = 1800 m s^{-1}, density = 2.0 g cm^{-3}, attenuation = 0.6 dB λ^{-1}).

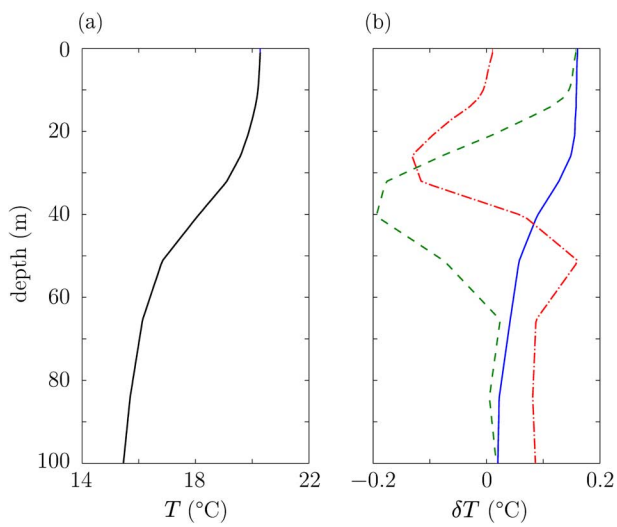

Fig. 7. Cabo Frio upwelling. (a) Mean profile of the ROMS temperature profiles at the defined offshore location. (b) First three EOFs of the same database (solid blue line: EOF 1; dashed green line: EOF 2; dashed–dotted red line: EOF 3).

The coastal sea bottom of Cabo Frio is modeled as a half-space of sand (compression wave speed = 1600 m s^{-1}, density = 1.8 g cm^{-3}, attenuation = 0.2 dB λ^{-1}). These geoacoustic

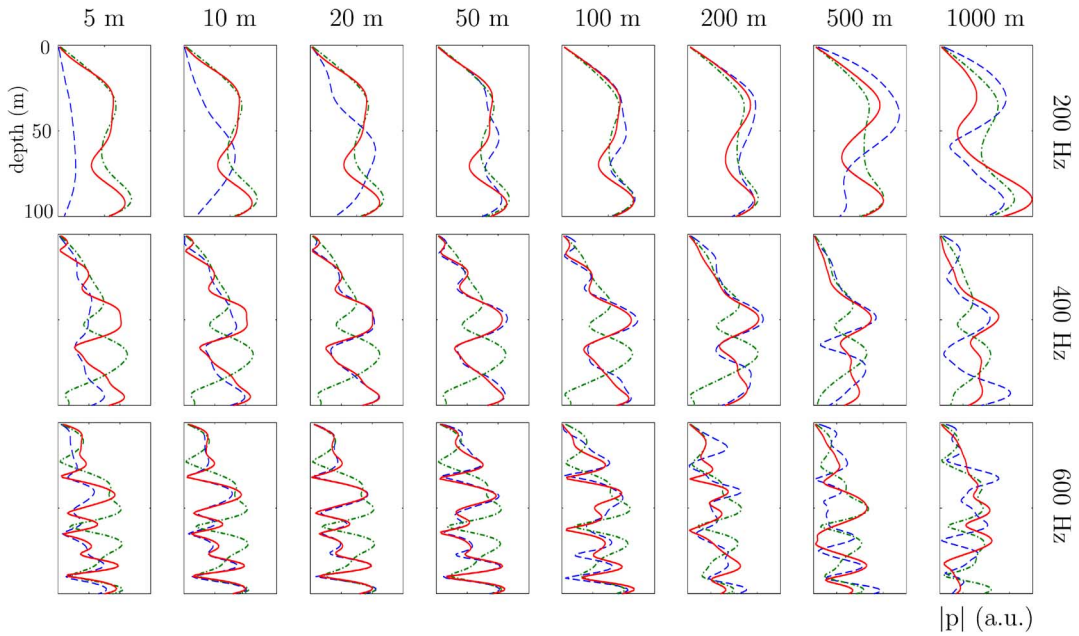

Fig. 8. Cabo Frio upwelling. Comparison of RAM (solid red), adiabatic KRAKEN (dashed–dotted green), and coupled KRAKEN (dashed blue) for the prediction of the pressure field amplitude at 200, 400, and 600 Hz (from top to bottom) as a function of depth, at 40-km range, for different horizontal resolutions (from left to right) of the temperature field constructed from an upwelling FM with ROMS-simulated inshore and offshore temperature profiles and a melt parameter a equal to 0 [central curve in Fig. 5(b)]. The acoustic source is placed inshore at 10-m depth. The pressure field amplitudes are normalized to 1 over the water depth to facilitate the comparison of the modal shapes obtained with the different models. The range discretization step used for RAM solution is the same for all tests, and is lower than the finest horizontal resolution of the temperature field [38].

models are based on the available data of both environments, but should be refined for real data inversion.

Different acoustic propagation models are compared for a typical upwelling situation modeled with the upwelling FM (Fig. 8). The water depth varies here continuously from 40 to 100 m. In the frequency range involved in this work (200–600 Hz, corresponding to wavelengths between 7.5 and 2.5 m), the range-dependent acoustic model (RAM) parabolic equation model [38] and the KRAKEN normal mode model (coupled-mode version) [39] are in good agreement provided that the horizontal discretization of the sound-speed field is sufficiently fine. For 200 Hz, the adiabatic normal mode propagation is sufficient to obtain a good correspondence with the parabolic approach. Numerical results with coupled-mode KRAKEN show that the optimal value for this discretization depends on the transmitted frequency, so that no discretization value is an optimum for the whole frequency band (exceeding an octave, in the present case). As expected, a coarse horizontal resolution implies larger variations in the sound-speed field, and can create artificial mode coupling that would not occur in the real environment. These results show the diminished reliability of coupled-mode prediction when the discretization of the sound-speed field is too fine (at least with the code used in this work). This effect is not observed with the adiabatic assumption or with the parabolic approach. Fig. 8 illustrates this observation. The origin of such an artifact has not been explored and is outside the scope of this paper. This undesirable feature incites the use of the RAM propagation model in the proposed application. However, for the frequency range used in this work (200–600 Hz) and the specific geometry involved in the simulations, a horizontal resolution of 100 m with a coupled normal mode approach gives satisfying results. In spite of a reduced accuracy, the coupled-mode KRAKEN is used in the remainder of the paper because of lower computational load.

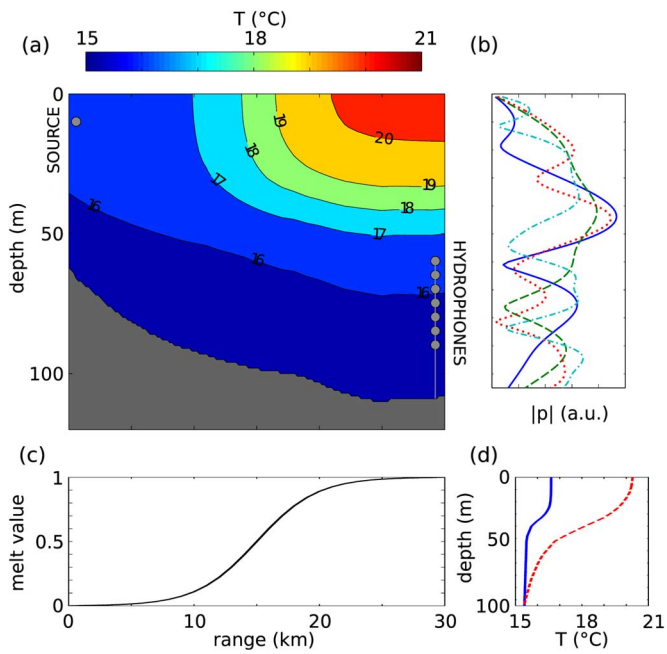

Fig. 9. Cabo Frio upwelling. (a) Reference temperature section constructed with the upwelling FM, using the melt function shown in (c) and the inshore profile (solid blue) and offshore profile (dashed red) shown in (d). The considered acoustic source and 16-element array setup is depicted. (b) Corresponding pressure field amplitude over the whole water column, located at 30 km from an acoustic source positioned at 10-m depth at the four third-octave frequencies [200 Hz (solid blue), 250 Hz (dashed green), 315 Hz (dotted red), and 400 Hz (dashed–dotted turquoise)].

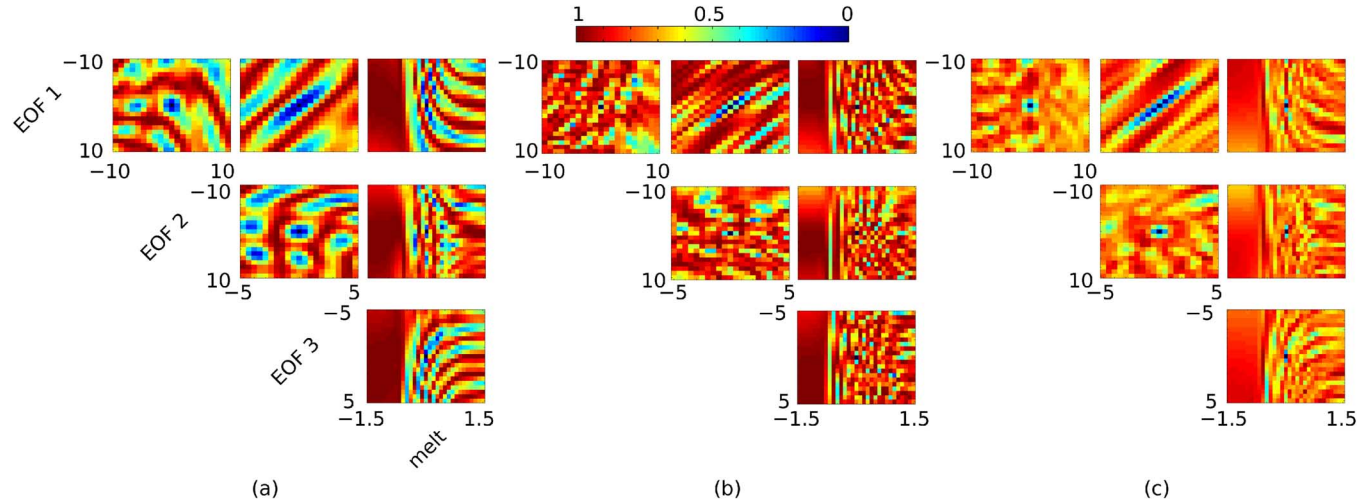

Fig. 10. Cabo Frio upwelling. Two-dimensional ambiguities for the upwelling FM parameters, using a source placed at 10-m depth, and a vertical array spanning the whole water column, for (a) a single frequency of 200 Hz, (b) a single frequency of 400 Hz, and (c) third-octave frequencies between 200 and 400 Hz. For each plot, two parameters vary, the other remaining fixed at their reference values.

B. Acoustic Sensitivity to Feature Model Parameters

The sensitivity of acoustic propagation to the feature-oriented parameterization is illustrated here for the upwelling front. The conventional (space-coherent) MFP objective function is computed for variations of the upwelling FM parameters around reference values. For the Ushant front, the reader is referred to [13], where objective function sensitivity to the Ushant front FM parameters is (partially) discussed.

The MFP objective function is defined as [40]

$$\phi(\boldsymbol{x}) = \frac{1}{N}\sum_{n=1}^{N} 1 - \frac{\boldsymbol{p}^{\dagger}(\boldsymbol{x},\omega_n) R(\omega_n) \boldsymbol{p}(\boldsymbol{x},\omega_n)}{\|\boldsymbol{p}(\boldsymbol{x},\omega_n)\|^2 \, \|\boldsymbol{d}(\omega_n)\|^2} \tag{5}$$

where $\boldsymbol{x}$ is the model vector (here, the FM parameters), $\boldsymbol{d}(\omega)$ is the vector of complex-valued acoustic-pressure measurements across the vertical array at the frequency ω, and $\boldsymbol{p}(\boldsymbol{x},\omega)$ is the corresponding predicted (replica) field vector of the complex-valued acoustic-pressure observations. $R(\omega)$ is the spatial correlation matrix at the frequency ω, defined as

$$R(\omega) = \boldsymbol{d}(\omega)\boldsymbol{d}^{\dagger}(\omega). \tag{6}$$

The † symbol denotes the conjugate transpose. Using (5), a value equal to 0 indicates the perfect match between data and replica and a value equal to 1 indicates completely uncorrelated measured and predicted values. The simultaneous use of several discrete frequencies is expected to enhance the tradeoff between robustness (lower frequencies) and sensitivity (higher frequencies).

The reference environment is constructed with the upwelling FM used in the inversion and tracking schemes. The inshore profile corresponds to a true profile from the oceanic numerical model ROMS. The offshore profile is a profile averaged on the whole set of temperature predictions at 30 km from the inshore profile. This profile corresponds to the mean profile of the EOF database (see Fig. 7), i.e., null EOF coefficients. The melt parameter is equal to 0. The corresponding temperature field and FM parameters are depicted in Fig. 9. The acoustic transmission is voluntarily kept in the lower frequency regime (between 200 and 400 Hz) to maintain a sufficiently high signal-to-noise ratio over the 30-km range of propagation, under real conditions. With a fixed inshore temperature profile the FM parameters are reduced to the melt parameter and three EOF coefficients for the offshore profile parameterization.

Figs. 10 and 11 show the values taken by the MFP objective function when varying two parameters simultaneously, with a fixed covariance matrix defined by acoustic propagation through the reference environment. In Fig. 10, a vertical array spanning the whole water column (1-m interelement spacing) is considered. Fig. 11 shows the corresponding ambiguities when reducing the array to 16 elements spanning 60–90-m water depths. The resulting ambiguities reveal a strong dependence in the number and range of frequencies involved in the objective function. Typically lower frequencies are less sensitive, but more robust to spatial inhomogeneities, and higher frequencies are more sensitive to spatial variations, thereby increasing the resolution of the estimates, but at the detriment of the robustness. This frequency-dependent feature is well observed comparing the ambiguities for a single frequency of 200 Hz (wide main lobe) and of 400 Hz (sharp mainlobe). A better tradeoff between uncertainty (large and low peaks) and sensitivity (sharp and high peaks) is realized when combining multiple frequencies. This compensation becomes more important when reducing the hydrophone array to a 16-element one (Fig. 11). Single-frequency ambiguities exhibit a large number of low secondary peaks that flatten out when increasing the number of frequencies inside the same band. It can be noted that the first and third EOFs show an important ambiguity that can be explained by their opposite trend in the 30–40-m depth interval [see Fig. 7(b)].

C. Coastal Feature Inversion and Sequential Tracking

The global minimum of the MFP objective function defined in (5) is searched using a global optimization approach, here

the differential evolution (DE) algorithm [41]. The DE algorithm attempts to progressively achieve the global minimum of the objective function by making populations of trial state vectors evolve (here, the FM parameters) through genetic-like combinations. Global optimization algorithms are often used for matched-field processing, since they enable a robust approach for solving the nonlinear objective functions which are typically multimodal (see, e.g., [40], [42], and [43]). Thus, for given acoustic measurements corresponding to a fixed environmental situation, the global optimization approach will find the vector of FM parameters that minimizes the mismatch with the prediction. For the purpose of continuous monitoring, global optimization methods are not appropriate, since they are typically expensive in terms of computational load and such a formulation does not take advantage of the continuous data stream. The inverse problem is then formulated in a Gauss–Markov state–space model [44], with a state vector $\boldsymbol{x}$ including the FM parameters and a measurement vector $\boldsymbol{y}$ including the acoustic measurements on the receiver array

$$\boldsymbol{x}(t_k) = \boldsymbol{\mathcal{A}}\left[\boldsymbol{x}(t_{k-1})\right] + \boldsymbol{w}(t_k) \qquad \text{[transition]} \qquad (7)$$

$$\boldsymbol{y}(t_k) = \boldsymbol{\mathcal{C}}\left[\boldsymbol{x}(t_k)\right] + \boldsymbol{v}(t_k) \qquad \text{[measurement]} \qquad (8)$$

where $\boldsymbol{w}(t_k)$ and $\boldsymbol{v}(t_k)$ are zero-mean Gaussian random vectors of covariance R_{ww} (process covariance) and R_{vv} (measurement covariance), respectively. The transition model $\boldsymbol{\mathcal{A}}$ describes the dynamics of the FM parameters, and is here simplified to an identity matrix, which reduces the transition model to a random walk for each state vector component, characterized by the process covariance. The state vector and the acoustic measurements are linked by a general nonlinear function $\boldsymbol{\mathcal{C}}$ that embeds the acoustic propagation model. As shown in [44], the use of a random walk model for the state vector can perform efficiently, provided that process covariance values are carefully adjusted and that new acoustic measurements are provided at a sufficient rate, to avoid strong environmental variations between successive data assimilations.

Under a Gaussian assumption, the sequential estimation of the state vector can be performed with a Kalman filter (KF) [45] that sequentially assimilates the data into the state–space model. The KF operates as a predictor/corrector algorithm. In the first step, the new state estimate $\hat{\boldsymbol{x}}(t_k|t_{k-1})$ [and its associated error covariance $\tilde{P}(t_k|t_{k-1})$] is predicted using the state–space model [see (7)]. In the second step, when measurements are available, the state estimate is corrected by the difference between the measurement predictions and the actual measurements weighted by the so-called Kalman gain K. The Kalman gain is computed at each new filtering step as a function of the measurement model, measurement covariance, and the previous value of the estimation error covariance.

A KF is tuned by adjusting the process and measurement covariance matrices R_{ww} and R_{vv}, respectively. Basically, it can be understood as follows: with small process noise covariance values, a large weight is given to the transition model (smaller Kalman gain). In contrast, small measurement noise covariance values will give greater confidence to the measurement model (larger Kalman gain). A proper tuning is thus required to obtain reliable estimates and meaningful statistics. In the present case of synthetic data, suitable covariance values can be deduced from statistics of the temperature field variations and errors in acoustic modeling due to the mismatch between the oceanic model scenario and the corresponding FM projection.

A nonlinear extension of KF is required to process the nonlinearity introduced by the measurement function [see (8)]. Here the extended Kalman filter (EKF [46]) was found to provide satisfying results. The EKF replaces the nonlinear function by a first-order Taylor series approximation leading to its Jacobian calculated around the last predicted state vector, keeping the matrix structure of the algorithm unchanged. The EKF algorithm is summarized in Table I.

When the nonlinearities are too strong, more advanced nonlinear KFs (unscented Kalman filter, ensemble Kalman filter) are used that do not involve a linearization step. Furthermore, if the probability distributions associated to the state or measurement parameters differ too much from a Gaussian distribution, numerical methods are required to fully characterize the non-Gaussian probability distribution. These methods are called particle filters (see, e.g., [47]).

The feature-oriented acoustic tomography (FOAT) approach is demonstrated in Sections IV and V on the two different front scenarios, extracted from a HYCOM simulation of the English Channel/Biscay system and from a ROMS simulation of the coastal area of Cabo Frio, respectively.

IV. Ushant Thermal Front Tracking

The first application proposed is the tracking of Ushant thermal front, and in particular its position, in a single vertical slice of the environment. The bathymetry is approximated by a flat bottom (offshore) of 110-m depth followed by a sloping bottom that extends to 65 m. The tide variations are not taken into account. A 16-element vertical array with 2-m interelement spacing spans the water column from 30 to 60 m and is placed inshore. An acoustic source at 5-m depth is chosen to mimic the acoustic center of ship machinery noise. Such a configuration is motivated by the development of bottom-mounted observatories, cable-connected to the shore, with the possible use of noise radiated by ships as acoustic source of opportunity, on the merchant traffic lanes that exist in the area (the so-called Ushant traffic separation scheme).

Fig. 12 shows the EKF tracking of the six front parameters during 48 h of acoustic data assimilation. For the first test, the acoustic data were synthesized from the projection of HYCOM model predictions on the FM parameter space (minimum RMSE on the 2-D temperature field). The resulting temperature variations (true parameters) can then be reproduced exactly if the correct FM parameter values are found by the tracker. Transmitted tones at three frequencies (200, 400, and 600 Hz) were jointly assimilated to perform the tracking. All FM parameters are well tracked, demonstrating the effectiveness of the random walk model on a trajectory which is not a random walk realization. The larger errors exhibited by the cold temperature parameter (F_c) tracking are explained by the weaker sensitivity of the measurements to this parameter. As explained above, on

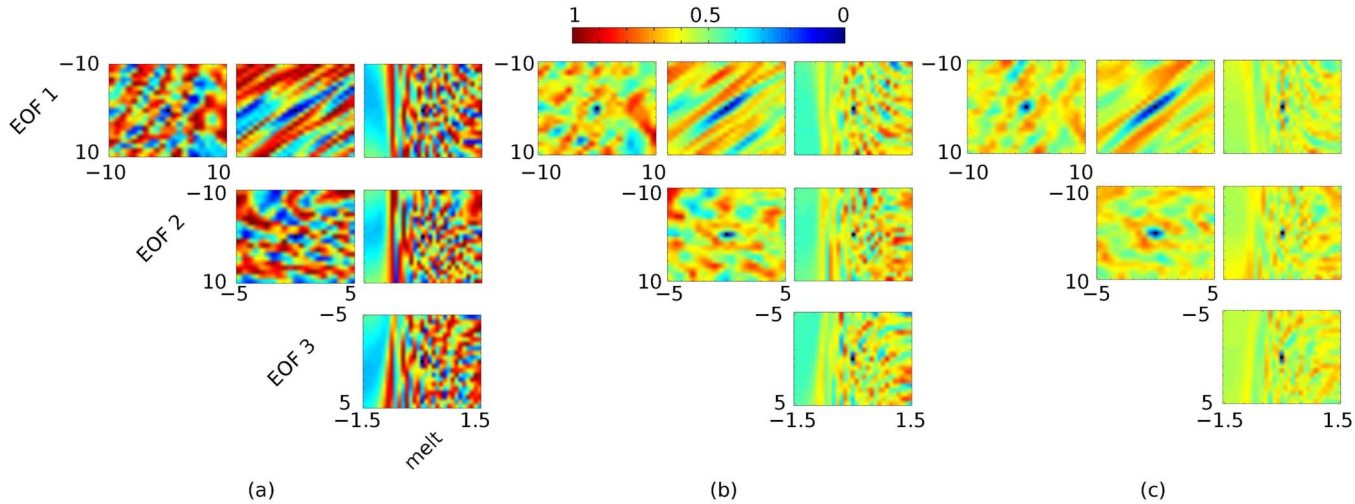

Fig. 11. Cabo Frio upwelling. Two-dimensional ambiguities for the upwelling FM parameters, using a 16-element array spanning 60–90-m water depths with (a) 400 Hz, (b) third-octave frequencies between 200 and 400 Hz, and (c) 12th-octave frequencies between 200 and 400 Hz.

TABLE I
EXTENDED KALMAN FILTER ALGORITHM IN A PREDICTION/CORRECTION FORM. THE DISCRETE TIME VARIABLE IS REDUCED TO THE INDEX k FOR THE SAKE OF CLARITY

Prediction	
$\hat{\boldsymbol{x}}(k\|k-1)=\boldsymbol{\mathcal{A}}[\hat{\boldsymbol{x}}(k-1\|k-1)]$	States
$\tilde{P}(k\|k-1)=A(k)\tilde{P}(k-1\|k-1)A(k)^T+R_{ww}$	States Cov.
$\hat{\boldsymbol{y}}(k\|k-1)=\boldsymbol{\mathcal{C}}[\hat{\boldsymbol{x}}(k\|k-1)]$	Measurements
Innovation	
$\boldsymbol{e}(k)=\boldsymbol{y}(k)-\hat{\boldsymbol{y}}(k\|k-1)$	Innovations
$R_{ee}(k)=C(k)\tilde{P}(k\|k-1)C(k)^T+R_{vv}$	Innov. Con.
Gain	
$K(k)=\tilde{P}(k\|k-1)C(k)^T R_{ee}^{-1}(k)$	Gain
Corection	
$\hat{\boldsymbol{x}}(k\|k)=\hat{\boldsymbol{x}}(k\|k-1)+K(k)\boldsymbol{e}(k)$	States
$\tilde{P}(k\|k)=[I-K(k)]\tilde{P}(k\|k-1)$	States Cov.
Initial Conditions	
$\hat{\boldsymbol{x}}(0),\tilde{P}(0)$	
Jacobians	
$A(k)=\left.\frac{\partial\boldsymbol{\mathcal{A}}(\boldsymbol{x})}{\partial\boldsymbol{x}}\right\|_{\boldsymbol{x}=\hat{\boldsymbol{x}}(k\|k-1)}, C(k)=\left.\frac{\partial\boldsymbol{\mathcal{C}}(\boldsymbol{x})}{\partial\boldsymbol{x}}\right\|_{\boldsymbol{x}=\hat{\boldsymbol{x}}(k\|k-1)}$	

this transect, the cold temperature parameter has a small effect on the acoustic propagation.

The second test involves acoustic data synthesized directly with the predictions of the HYCOM model, i.e., without a preliminary projection on the FM parameter space. Such a test confirms that the simplified FM parameterization is sufficient to reproduce the principal characteristics of the acoustic propagation into a realistic oceanic model. As expected, the performances are deteriorated, but the principal parameter (the front position r_0) is roughly tracked during 40 h, before diverging, when the model mismatch becomes significant. This tracking has been realized with 16 frequencies, from 200 to 500 Hz with a step of 20 Hz, as an attempt to increase the robustness of the filter.

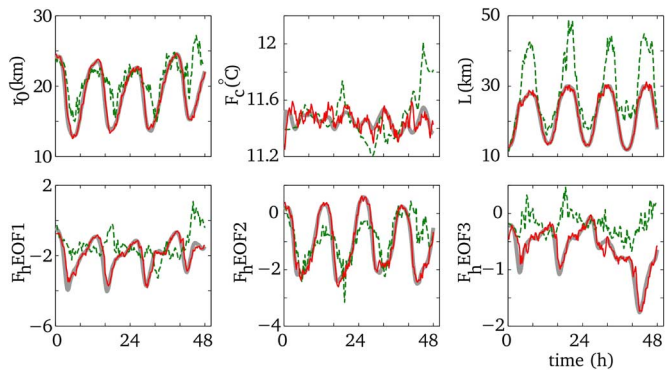

Fig. 12. Ushant thermal front. EKF tracking based on the assimilation of 15-min spaced acoustic data. Projection of the HYCOM model on the FM parameter space (thick gray), tracking of the reproducible scenario (solid red), and tracking of the true HYCOM predictions (dashed green).

Different features cannot be reproduced by the FM, especially the upwelling and mixing of water near the coast, but the global structure of the front is well tracked. A more complex FM, e.g., with a second EOF parameterization for the cold profile, might enhance the quality of the temperature field reconstruction, and consequently the robustness of the filtering scheme.

From the oceanographic viewpoint, the performance of the filter has to be translated in terms of errors on the temperature field estimation. Fig. 13 compares the RMSE on the temperature field estimates for a different number of frequencies transmitted in the environment. Each tracking test was run 30 times with a different noise realization on the acoustic pressure field and different initial conditions to initialize the filter. Five sets of frequencies have been tested. The tests with the single frequency of 200 or 600 Hz show divergence in the tracking as indicated by an error continuously increasing with time. The cause of such a divergence is explained differently for the two frequencies. A frequency too low (200 Hz) is not sufficiently sensitive to the slow variations in the range dependence of the sound-speed field. On the other hand, at higher frequencies (here, 600 Hz), slight variations in the sound-speed field have a strong effect on the acoustic propagation. The frequency of 400 Hz seems to

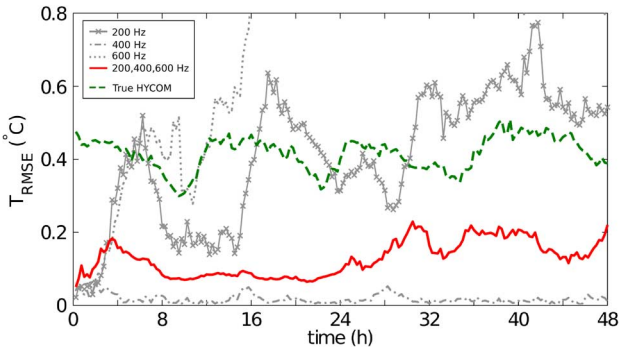

Fig. 13. Ushant thermal front. Evolution of the range- and depth-averaged RMSE on the temperature field for FM-synthesized acoustic data. The RMSE obtained with the tracking of the true HYCOM prediction is shown for comparison.

realize the tradeoff between both types of sensitivity resulting in a stable tracking performance. The joint filtering of several frequencies enhances the tracking results when using the lower frequencies of 200 and 400 Hz (not shown). However, the additional inclusion of the higher frequency of 600 Hz as a third observable slightly degrades the tracking performance. The RMSE obtained with the tracking of the true HYCOM predictions is shown in Fig. 13. Its value follows closely the minimum achievable value with the FM parameterization (not shown). The divergence of the front position parameter r_0 (Fig. 12) is not reflected in the RMSE, showing that the filter itself is not diverging.

Simulation results show the ability of full-field acoustic tomography to provide an additional monitoring tool for the Ushant tidal front. Application of this scheme on realistic temperature predictions from a numerical oceanic model gives encouraging results, with a reasonable tracking of the main structure of the front. The assimilation of multiple frequencies is shown to enhance the performances of the filter but assimilated frequencies have to be maintained in the low range (lower than 600 Hz) to avoid oversensitivity to sound-speed field perturbations.

V. Cabo Frio Upwelling Tracking

The second application is the detection and tracking of the upwelling in a single vertical slice of the coastal area of Cabo Frio.

A. Upwelling Global Optimization

Two different situations are tested with the DE global optimization algorithm. The first temperature field corresponds to a quasi-stratified situation [Fig. 14(a)] and the second corresponds to an upwelling situation [Fig. 14(b)]. Both temperature sections are extracted from the ROMS simulation. The pressure field data are synthesized directly from these two outputs of the ROMS model, without preliminary projection on the FM parameter space, at the four third-octave frequencies in the band 200–400 Hz, and acquired on a vertical array spanning the whole water column.

The DE algorithm is used here with 32 individuals (parameter vectors) that evolve along 300 generations. Increased populations were not found to enhance the results. As expected, the parameterization scheme is much more efficient for the upwelling

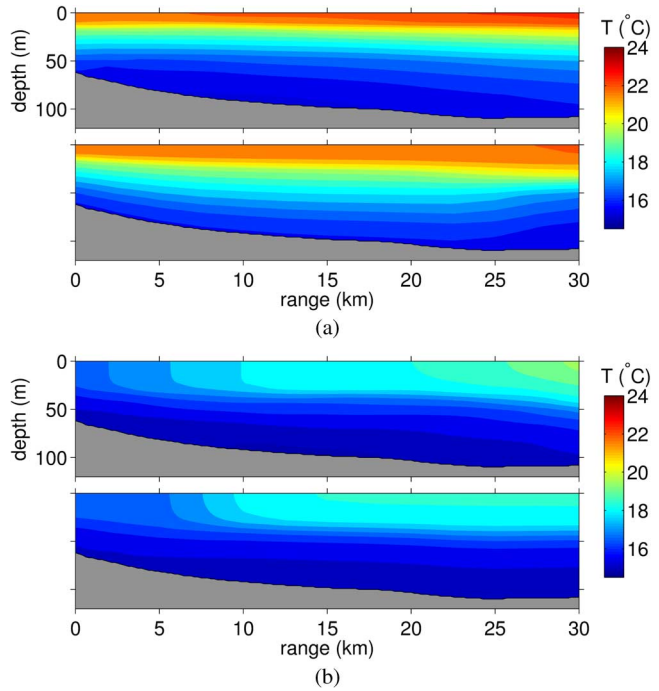

Fig. 14. Cabo Frio upwelling. (a) Quasi-stratified temperature field simulated with the ROMS model (top) and its FM estimate obtained by inversion of the multiple-frequency acoustic data (200, 250, 315, and 400 Hz) (bottom). (b) Upwelling temperature field simulated with the ROMS model (top) and its FM estimate obtained by inversion of the multiple-frequency acoustic data (bottom).

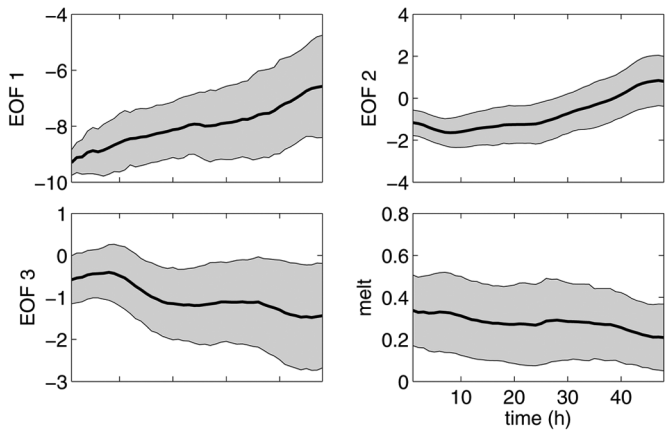

Fig. 15. Cabo Frio upwelling. Averaged upwelling FM parameter sequential tracking (black) over 50 EKF realizations and corresponding standard deviation (gray).

situation. In fact, the first situation is more efficiently modeled by a range-averaged sound-speed profile, since no strong range dependency of the temperature field exists. However, it demonstrates that the feature-oriented parameterization scheme can still be maintained in a situation where cold waters are not strongly upwelled and does not produce unphysical solutions. The range- and depth-integrated RMSE on the temperature field is equal to 0.77 °C, with an associated MFP objective value of 0.50, in the stratified case, while the RMSE on the temperature field is reduced to 0.25 °C, with an associated MFP objective value of 0.20, for the upwelling situation. In both situations, the RMSE remains in the range of the error obtained with the direct comparison of oceanic outputs and FM representations (i.e., without any acoustic inversion).

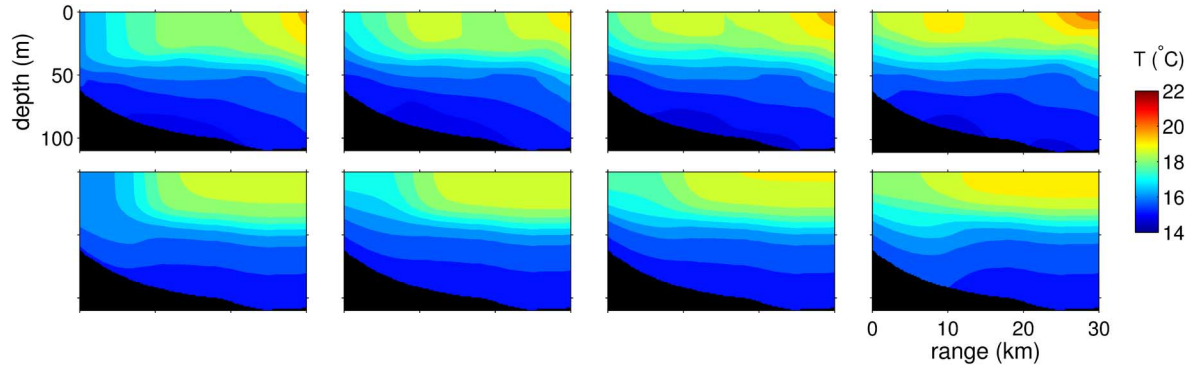

Fig. 16. Cabo Frio upwelling. Evolution of the 2-D temperature field predicted by the ROMS model (top) and the EKF averaged estimates (bottom) after 12, 24, 36, and 48 h (from left to right). The oceanic bottom is represented in black.

B. Upwelling Sequential Tracking

We consider now 48 h of predictions extracted from the ROMS simulation of the Cabo Frio area, starting from the situation of upwelled waters shown in Fig. 14(b). For every new temperature field prediction, acoustic pressure field data are synthesized at the four third-octave frequencies between 200 and 400 Hz on a vertical array of hydrophones spanning the whole water column, so that 48 successive hours of acoustic data are available for filtering, with new data every hour. Fig. 15 shows the evolution of the averaged estimates over 50 EKF tracking realizations and the associated spread (one standard deviation). Each EKF realization differs in its initial conditions. The progressive increase of the first EOF coefficient is related to the increase of the offshore surface temperature, while the second EOF coefficient reinforced the thermocline gradient. The (slight) decrease of the melt parameter can be associated to the progressive weakening of the upwelling feature.

The temperature field evolution and its reconstruction from the averaged estimates over the EKF realizations are illustrated in Fig. 16. Localized temperature perturbations cannot be reproduced by the FM, but the main structure is shown to be tracked. This is confirmed by the range- and depth-integrated RMSE between the original temperature field and the reconstructed field (Fig. 17). The RMSE is stable and remains in the range of the FM accuracy, since the maximum value is equal to 0.35 °C. This means that the acoustic data filtering is sufficient to maintain a stable estimate of the range-dependent temperature field, even if nonreproducible inhomogeneities exist in the true oceanic scenario. The RMSE for EKF filtering of single-frequency data (200 and 400 Hz) shows similar performances for these first 48 h. However, the filtering of 48 additional hours results in a lower RMSE for the multiple frequency data (Fig. 17). The highest RMSEs are found for the highest frequency data filtering (400 Hz).

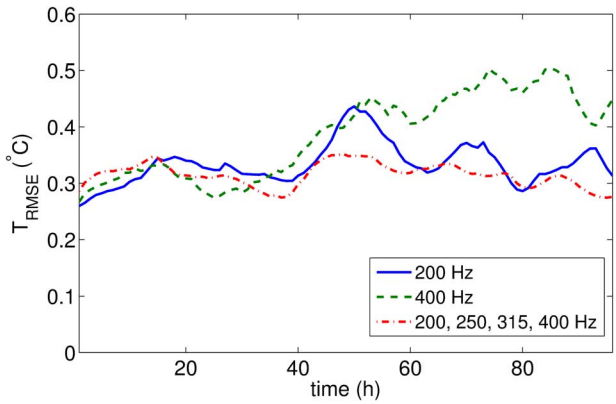

Fig. 17. Cabo Frio upwelling. Evolution of the range- and depth-averaged RMSE on the temperature field between ROMS simulation and EKF estimates. Each curve involves a different frequency setup for the tracking.

VI. Conclusion and Perspectives

The use of feature modeling is proposed for the acoustic characterization of 2-D range-dependent temperature fields (vertical slices). Based on a simple geometrical description of an identified oceanographic feature, here coastal thermal fronts, the so-called feature model (FM) approximates the temperature field with a low-dimensional state vector. The dimension of the parameter space is, therefore, reduced to the description of the two extreme vertical profiles and a suitable parameterization of the transition between them. In this work, an EOF parameterization is proposed for the offshore profiles, but any other parameterization can be developed since it is independent of the FM geometrical construction itself.

Two well-known coastal front cases serve to test the use of FM for range-dependent acoustic tomography. The first front is the Ushant front which is a tidal front appearing almost every year during the northern summer in the Iroise sea. Oceanic circulation models provide realistic variable temperature fields for testing the tracking of vertical slices of the front through full-field acoustic inversion. The second case is the upwelling front of the coastal area off Cabo Frio, which is more frequently observed during the austral summer. The impact of these two oceanographic features on the biological resources and the complex coupling of the underlying processes with the open ocean motivates the development of efficient observational methods for data assimilation.

The concept of FOAT is demonstrated here on realistic temperature variations in vertical slices of Ushant and Cabo Frio areas. The temperature variations are obtained with validated regional oceanic model simulations. Both a global inversion algorithm (genetic algorithm) and a sequential filtering method (Kalman filter) were applied on synthetic acoustic pressure field data on a vertical array of hydrophones in two possible configurations for the development of long-term observatories. In

Ushant area, a bottom-moored hydrophone array is cabled inshore and records pressure field data from a shallow acoustic source offshore. The monitoring of the coastal upwelling in Cabo Frio is realized with a shallow acoustic source, cabled inshore, and a bottom-moored array of hydrophone a few tens of kilometers offshore. This approach constitutes an interesting way to monitor acoustically the 3-D volume of the environment by combining multiple slices defined by the source–receiver pairs.

Sequential Bayesian tracking provided here by KF algorithm, enables continuous tracking of the FM parameters by sequentially inverting successive full-field acoustic data on the array of hydrophones. For the two different configurations, FOAT provides estimation errors on the same order as the respective FM approximation errors. The simultaneous filtering of several frequencies is shown to enhance the accuracy of the estimates and the robustness of the filter. Range-dependent sensitivity issues, coupled-mode propagation, and midrange propagation force consideration of acoustic frequencies in the range of 200–500 Hz, which is suited well with the possible use of radiated ship noise. The proposed scheme can be further improved by considering multiple vertical slices to estimate 3-D fields, or by assimilating different types of measurements (*in situ*, satellite).

In the future, merchant ships on the Ushant traffic lanes (see Fig. 1) can serve as source of opportunity enabling the inversion and tracking of the radiated noise and spectral lines. Long-term passive acoustic data collected on AURAL autonomous hydrophones deployed in 2009 and 2010 near the traffic lanes will serve to study inversion techniques for coastal tomography in this area, together with the feature-oriented approach. Acoustic data acquired in Cabo Frio area during the 2010 Ocean Acoustic Exploration IRSES (OAEx) experiments [48] will serve to test FOAT performances in a real active configuration.

ACKNOWLEDGMENT

The authors would like to thank Y. Stéphan and L. Calado for providing the HYCOM and ROMS simulation data, and L. Ponsoni and J. Randall from the Acoustics & Environmental Hydroacoustics Lab, Université libre de Bruxelles (ULB), Brussels, Belgium, for help in preparing graphics and proofreading the revised manuscript.

REFERENCES

[1] P. Lermusiaux and C. S. Chiu, "Four-dimensional data assimilation for coupled physical-acoustical fields," in *Acoustic Variability 2002*, N. Pace and F. Jensen, Eds. Norwell, MA: Kluwer, 2002, pp. 417–424.

[2] P. Elisseeff, H. Schmidt, and W. Xu, "Ocean acoustic tomography as a data assimilation problem," *IEEE J. Ocean. Eng.*, vol. 27, no. 2, pp. 275–282, Apr. 2002.

[3] W. Munk and C. Wunsch, "Ocean acoustic tomography: A scheme for large scale monitoring," *Deep-Sea Res.* vol. 26, no. 2, pp. 123–161, 1979 [Online]. Available: http://dx.doi.org/10.1016/0198-0149(79)90073-6

[4] L. R. LeBlanc and F. H. Middleton, "An underwater acoustic sound velocity data model," *J. Acoust. Soc. Amer.*, vol. 67, no. 6, pp. 2055–2062, 1980.

[5] T. Itoh, T. Kamoshida, T. Shinke, N. Kimata, and A. Kaya, "1000-km range 2 dimensional ocean acoustic tomography near Japan," in *Proc. MTS/IEEE OCEANS Conf., Challenges of Our Changing Global Environ.*, 1995, vol. 3, pp. 1459–1468.

[6] M. I. Taroudakis and M. G. Markaki, "On the use of matched-field processing and hybrid algorithms for vertical slice tomography," *J. Acoust. Soc. Amer.*, vol. 102, no. 2, pp. 885–895, 1997.

[7] V. Corré and S. M. Jesus, "Tracking of cold water upwelling filaments in the ocean using matched field inversion," *Acta Acustica United Acustica*, vol. 89, pp. 604–613, 2003.

[8] O. Carrière, J.-P. Hermand, and J. V. Candy, "Inversion for time-evolving sound-speed field in a shallow ocean by ensemble Kalman filtering," *IEEE J. Ocean. Eng.*, vol. 34, no. 4, pp. 586–602, Oct. 2009.

[9] T. H. Rousseau, W. L. Siegmann, and M. J. Jacobson, "Acoustic propagation through a model of shallow fronts in the deep ocean," *J. Acoust. Soc. Amer.*, vol. 72, no. 3, pp. 924–936, 1982.

[10] A. D. Heathershaw, C. E. Stretch, and S. J. Maskell, "Coupled ocean-acoustic model studies of sound propagation through a front," *J. Acoust. Soc. Amer.*, vol. 89, no. 1, pp. 145–155, 1991.

[11] G. Jin, J. F. Lynch, C. S. Chiu, and J. H. Miller, "A theoretical and simulation study of acoustic normal mode coupling effects due to the Barents sea polar front, with applications to acoustic tomography and matched-field processing," *J. Acoust. Soc. Amer.*, vol. 100, no. 1, pp. 193–205, 1996.

[12] R. Field, M. Broadhead, and G. Peggion, "The effects of a dynamic shallow water front on acoustic propagation," in *Proc. IEEE OCEANS Conf.*, 1998, pp. 209–213.

[13] O. Carrière, J.-P. Hermand, and Y. Stéphan, "Passive tomography in coastal areas: A feasibility study of the Ushant front monitoring," in *Proc. New Trends for Environm. Monitor. Using Passive Syst.*, Hyères, France, Oct. 2008, DOI: 10.1109/PASSIVE.2008.4786979.

[14] J. Small, L. Shackleford, and G. Pavey, "Ocean feature models—Their use and effectiveness in ocean-acoustic forecasting," *Ann. Geophysicae*, vol. 15, pp. 101–112, 1997.

[15] A. Gangopadhyay and A. R. Robinson, "Feature-oriented regional modeling of oceanic fronts," *Dynam. Atmos. Oceans*, vol. 36, pp. 201–232, 2002.

[16] L. Calado, A. Gangopadhyay, and I. C. A. Silveira, "Feature-oriented regional modeling and simulations (FORMS) for the western south Atlantic: Southeastern Brazil region," *Ocean Model.*, vol. 25, pp. 48–64, 2008.

[17] L. Calado, A. Gangopadhyay, and I. C. A. Silveira, "A parametric model for the Brazil Current meanders and eddies off southeastern Brasil," *Geophys. Res. Lett.*, vol. 33, 2006, LI2602.

[18] G. R. Halliwell, R. Bleck, and E. Chassignet, "Atlantic ocean simulations performed using a new hybrid-coordinate ocean model," in *Proc. EOS Fall AGU Meeting*, 1998, OS12D-03.

[19] D. Haidvogel, H. Arango, W. Budgell, B. Cornuelle, E. Curchitser, E. Di Lorenzo, K. Fennel, W. Geyer, A. Hermann, and L. Lanerolle, "Ocean forecasting in terrain-following coordinates: Formulation and skill assessment of the Regional Ocean Modeling System," *J. Comput. Phys.*, vol. 227, no. 7, pp. 3595–3624, 2008.

[20] S. M. Jesus, C. Soares, E. Ferreira-Coelho, and P. Picco, "An experimental demonstration of blind ocean acoustic tomography," *J. Acoust. Soc. Amer.*, vol. 119, no. 3, pp. 1420–1431, 2006.

[21] A. V. van Leijen, J.-P. Hermand, and M. Meyer, "Geoacoustic inversion in the north-eastern Caribbean using a hydrographic survey vessel as a sound source of opportunity," *J. Mar. Syst.*, vol. 78, pp. S333–S338, 2009.

[22] S. Vallez, C. Gervaise, A. Khenchaf, Y. Stephan, and M. Andre, "Passive geoacoustic inversion of very shallow water environment with ship's noise: Incoherent processing," *Traitement du Signal*, vol. 25, no. 1–2, pp. 151–163, 2008.

[23] Y. Stéphan, J.-P. Hermand, and O. Carrière, "Operational feasibility of an acoustic passive monitoring of the Ushant front," in *Proc. 3rd Int. Conf. Exhibit. Underwater Acoust. Meas., Technol. Results*, J. S. Papadakis and L. Bjorno, Eds., Nafplion, Greece, Jun. 2009.

[24] J.-P. Hermand, "Broad-band geoacoustic inversion in shallow water from waveguide impulse response measurements on a single hydrophone: Theory and experimental results," *IEEE J. Ocean. Eng.*, vol. 24, no. 1, pp. 41–66, Jan. 1999.

[25] Z. Michalopoulou, "Matched-impulse-response processing for shallow-water localization and geoacoustic inversion," *J. Acoust. Soc. Amer.*, vol. 108, no. 5, pp. 2082–2090, 2000.

[26] J.-C. Le Gac, M. Asch, Y. Stephan, and X. Demoulin, "Geoacoustic inversion of broad-band acoustic data in shallow water on a single hydrophone," *IEEE J. Ocean. Eng.*, vol. 28, no. 3, pp. 479–493, Jul. 2003.

[27] SHOM-METEO, "Atlas de fronts thermiques en Atlantique Nord Est d'après l'imagerie satellitale," Service Hydrographique et Océanographique de la Marine (SHOM), Tech. Internal Rep. R/1765.1&2B, 1996.
[28] Y. Stéphan and C. Gervaise, *Personal Communication.* 2010.
[29] R. Bleck, "Ocean modeling in isopycnic coordinates," in *Ocean Modeling and Parameterization*, ser. NATO Science Series, E. P. Chassignet and J. Verron, Eds. Amsterdam, The Netherlands: Springer-Verlag, 1998, vol. 516, pp. 423–448.
[30] Y. Morel, A. Pichon, S. Louazel, L. Pineau-Guillou, R. Baraille, A. Serpette, C. Lathuilière, F. Ardhuin, A. Pasquet, S. Correard, M. Assenbaum, S. Casitas, L. Quaresma Dos Santos, C. Renaudie, G. Hello, H. Giordani, S. Lahaye, and X. Carton, "Modélisation de la circulation océanique en Manche, Golfe de Gascogne, Ouest-Portugal et Golfe de Cadix," *Ann. Hydrographiques*, vol. 6, no. 775, pp. 3.1–3.15, 2010.
[31] Sociétés Géosciences Ingénierie and ACTIMAR, "Projet HYCOMANE, Maquette Gascogne-Manche, simulations sur l'année," Tech. Rep., 2005.
[32] R. R. Rodrigues and J. A. Lorenzzetti, "A numerical study of the effects of bottom topography and coastline geometry on the Southeast Brazilian coastal upwelling," *Continental Shelf Res.*, vol. 21, pp. 371–394, 2001.
[33] L. Calado, I. C. A. da Silveira, A. Gangopadhyay, and B. M. de Castro, "Eddy-induced upwelling off Cape of São Tomé (22° S, Brazil)," *Continental Shelf Res.*, vol. 30, no. 10–11, pp. 1181–1188, 2010.
[34] O. Carrière, J.-P. Hermand, L. Calado, A. C. de Paula, and I. C. A. da Silveira, "Feature-oriented acoustic tomography: Upwelling at Cabo Frio (Brazil)," in *Proc. MTS/IEEE OCEANS Conf., Marine Technology for Our Future: Global and Local Challenges*, Biloxi, MS, Oct. 2009, pp. 1–8.
[35] C. Shaji and A. Gangopadhyay, "Synoptic modeling in the eastern Arabian Sea during the southwest monsoon using upwelling feature models," *J. Atmos. Ocean. Technol.*, vol. 24, pp. 877–893, 2007.
[36] National Centers for Environmental Prediction [Online]. Available: http://www.ncep.noaa.gov/
[37] N. R. Chapman, S. Chin-Bing, D. King, and R. B. Evans, "Benchmarking geoacoustic inversion methods for range-dependent waveguides," *IEEE J. Ocean. Eng.*, vol. 28, no. 3, pp. 320–330, Jul. 2003.
[38] M. D. Collins, "User's guide for RAM versions 1.0 and 1.0p," 1999 [Online]. Available: ftp://ftp.ccs.nrl.navy.mil/pub/ram/RAM/
[39] M. B. Porter, "The KRAKEN normal mode program," 1997 [Online]. Available: http://oalib.hlsresearch.com/Modes/kraken.pdf
[40] J.-P. Hermand and P. Gerstoft, "Inversion of broad-band multitone acoustic data from the Yellow Shark summer experiments," *IEEE J. Ocean. Eng.*, vol. 21, no. 4, pp. 324–346, Oct. 1996.
[41] R. Storn and K. Price, "Differential evolution—A simple and efficient heuristic for global optimization over continuous spaces," *J. Global Optim.*, vol. 11, no. 4, pp. 341–359, 1997.
[42] M. D. Collins, W. A. Kuperman, and H. Schmidt, "Nonlinear inversion for ocean-bottom properties," *J. Acoust. Soc. Amer.*, vol. 92, no. 5, pp. 2770–2783, 1992.
[43] P. Gerstoft, "Inversion of seismoacoustic data using genetic algorithms and a posteriori probability distributions," *J. Acoust. Soc. Amer.*, vol. 95, no. 2, pp. 770–782, 1994.
[44] O. Carrière, J.-P. Hermand, J.-C. Le Gac, and M. Rixen, "Full-field tomography and Kalman tracking of the range-dependent sound speed field in a coastal water environment," *J. Mar. Syst.*, vol. 78, Special Issue on MREA and Coastal Processes: Challenges for Monitoring and Prediction, pp. S382–S392, 2009.
[45] R. E. Kalman, "A new approach to linear filtering and prediction problems," *J. Basic Eng. D*, vol. 82, pp. 35–45, 1960.
[46] , A. Gelb, Ed., *Applied Optimal Estimation*. Cambrige, MA: MIT Press, 1974, ch. 6.
[47] J. V. Candy, *Bayesian Signal Processing: Classical, Modern, and Particle Filtering Methods*. New York: Wiley/IEEE Press, 2009, ch. 7.
[48] European Commission, "Ocean Acoustic Exploration IRSES (OAEx)," Eur. 7th Framework Programs.

Olivier Carrière received the M.S. degree in physics and the Ph.D. degree in sciences from the Faculty of Sciences, Université libre de Bruxelles (ULB), Brussels, Belgium, in 2006 and 2011, respectively. His Ph.D. research was focused on the development of sequential Bayesian techniques for solving acoustic tomography and geoacoustic inversion problems in shallow-water and coastal environments, supervised by Prof. J.-P. Hermand.

Currently, he is a Postdoctoral Researcher at the Marine Physical Laboratory, Scripps Institution of Oceanography, University of California, San Diego. His research interests are noise processing, sequential filtering methods, underwater acoustic inversion, reflection seismology, and underwater imaging techniques.

Jean-Pierre Hermand (M'86–SM'05–F'09) received the Ingénieur Civil degree in electrical and mechanical engineering and the Ph.D. degree in applied sciences from the Université libre de Bruxelles (ULB), Brussels, Belgium, in 1981 and 1994, respectively.

Between 1985 and 2000, he has held several positions at the SACLANT Undersea Research Centre, La Spezia, Italy, conducting experimental and theoretical research in ocean acoustics with emphasis on inverse problems. In 1991, he became the Principal Investigator of a grant from the U.S. Office of Naval Research to develop environmentally adaptive sonar processing at the Naval Underwater Systems Center, New London, CT. In 1993, he was appointed Principal Scientist to the SACLANTCEN Environmental Research Division to lead the research and development of acoustic sensing techniques and inversion methodologies for the characterization of shallow-water marine sediments. He has been a Scientist-in-Charge for multidisciplinary and exploratory experiments at sea. Currently, he is Professor and Research Director at the Université libre de Bruxelles, where he founded the Environmental Hydroacoustics Laboratory. Since 2001, he has been providing leadership for cross-disciplinary research on ocean acoustic observatories in the framework of European and international projects. His current research interests lie in the integrated use of acoustics in underwater geosciences, in particular to remotely sense dynamics of ocean fronts, productivity in marine habitats, Stone Age culture layer, and sediment processes in river and estuary.

Dr. Hermand is a Fellow of the Acoustical Society of America and a member of the IEEE Societies of Oceanic Engineering (OES) and Signal Processing (SPS). He is currently the Chair of the IEEE/OES Technical Committee on "Ocean Signal and Image Processing" and Elected Member of OES Administrative Committee.